CHEMISTRY OF MATERIALS
Cite This: Chem. Mater. 2017, 29, 9407-9415
Article
pubs.acs.org/cm

Importance of 2D Conjugated Side Chains of Benzodithiophene-Based Polymers in Controlling Polymer Packing, Interfacial Ordering, and Composition Variations of All-Polymer Solar Cells

Changyeon Lee,[†] Thota Giridhar,[†] Joonhyeong Choi,[†] Seonha Kim,[†] Youngwoong Kim,[†] Taesu Kim,[†] Wonho Lee,[†] Han-Hee Cho,[†] Cheng Wang,[‡] Harald Ade,[§] and Bumjoon J. Kim*[,†]

[†]Department of Chemical and Biomolecular Engineering, Korea Advanced Institute of Science and Technology (KAIST), Daejeon 34141, Republic of Korea

[‡]Advanced Light Source, Lawrence Berkeley National Laboratory, Berkeley, California 94720, United States

[§]Department of Physics and Organic and Carbon Electronics Laboratory, North Carolina State University, Raleigh, North Carolina 27695, United States

Supporting Information

ABSTRACT: We delineate the important role of 2D conjugated alkylthiophene side chains of polymers in manipulating the molecular orientation and ordering at the polymer donor/polymer acceptor (P_D/P_A) interface as well as the composition variations in the blend active layer of all-polymer solar cells (all-PSCs). To systematically investigate the impact of 2D conjugated side chains on the performance of all-PSCs, we synthesized a series of poly(benzo[1,2-*b*:4,5-*b*̀]-dithiophene-thieno[3,4-*c*]pyrrole-4,6-dione) (PBDTTPD) polymer donors with different contents of alkoxy and alkylthiophene side chains, from 0 to 100% (PBDT-TPD (**P1**, 100% alkoxy side chain), $PBDTT_{0.29}$-TPD (**P2**), $PBDTT_{0.59}$-TPD (**P3**), $PBDTT_{0.76}$-TPD (**P4**), and PBDTT-TPD (**P5**, 100% alkylthiophene side chain). The **P1**−**P5** polymer donors produced similar PCEs of ∼6% in fullerene-based PSCs. In contrast, for the all-PSC systems, the changes in the side chain composition of the polymers induced a strong increasing trend in the power conversion efficiencies (PCEs), from 2.82% (**P1**), to 3.16% (**P2**), to 4.41% (**P3**), to 5.32% (**P4**), and to 6.60% (**P5**). The significant increase in the PCEs of the all-PSCs was attributed mainly to improvements in the short-circuit current density (J_{SC}) and fill factor (FF). The 2D conjugated side chains promoted localized molecular orientation and ordering relative to the P_D/P_A interfaces and improved domain purity, which led to enhanced exciton dissociation and charge transport characteristics of the all-PSCs. Our observations highlight the advantage of incorporating 2D conjugated side chains into polymer donors for producing high-performance all-PSC systems.

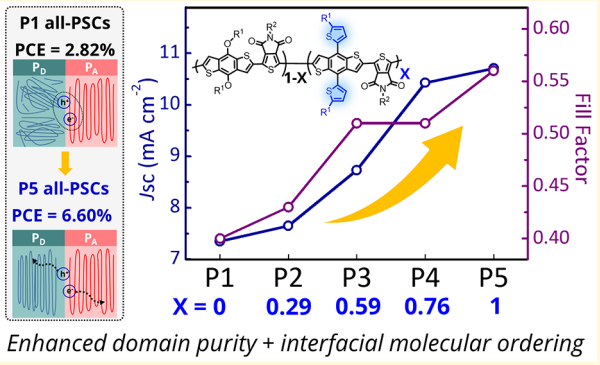

INTRODUCTION

All-polymer solar cells (all-PSCs), in which the active layer consists of both an electron-donating polymer (P_D) and an electron-accepting polymer (P_A), have gained growing interest because of their promising advantages including enhanced complementary light absorption from the P_D and P_A components, facile tunability of energy levels of P_D and P_A, and high thermal/mechanical stability.[1−3] The power conversion efficiencies (PCEs) of all-PSCs have improved significantly in a brief span of years, with PCEs now in the range of 7−9%.[3−22] This rapid progress has been made possible by the effective use of the strategies developed and the lessons learned in extensive studies of fullerene-based PSCs. For example, one of the major hurdles limiting the PCEs of all-PSCs, that is, undesirable large-scale phase separation of polymer blends in bulk-heterojunction (BHJ) layers, was improved in part by approaches used frequently to increase the efficiency of polymer/fullerene solar cell (fullerene-PSC) systems. These approaches include controlling the molecular weight and side chains of the polymer components[4,23−32] and the use of P_D/P_A pairs with low interfacial tension.[33]

One intriguing and important issue remains to be addressed, particularly for the design of high-performance all-PSCs. Unlike fullerene acceptors that have ball-like symmetric molecular geometry (e.g., phenyl-C_{61}-butyric acid methyl ester (PCBM)), P_As have highly anisotropic (planar) conjugated chemical structures.[24,34] This feature associated with P_As often hampers efficient charge separation of Coulombically bound excitons at the P_D/P_A interface of all-polymer blends due to the lack of face-to-face alignment of P_D and P_As desire to afford

Received: August 18, 2017
Revised: September 26, 2017
Published: October 11, 2017

DOI: 10.1021/acs.chemmater.7b03495
Chem. Mater. 2017, 29, 9407−9415

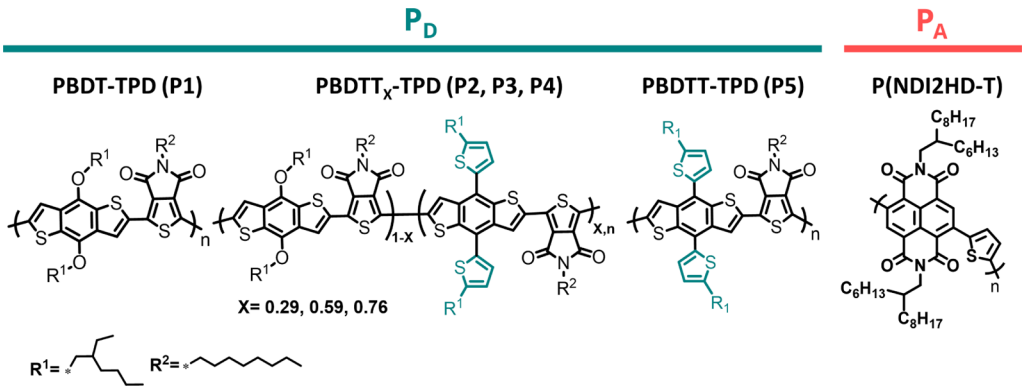

Figure 1. Chemical structures of the polymer donors (**P1**−**P5**) and polymer acceptor (P(NDI2HD-T)) used in this study.

Table 1. Properties of P1−P5

	BDT:BDTT						
P_D	feed ratio	actual ratio[a]	M_n (kg/mol)[b]	$Đ$ (M_w/M_n)[b]	E^{opt} (eV)[c]	HOMO (eV)[d]	LUMO (eV)[e]
P1	1:0	1:0	28.8	1.9	1.86	−5.44	−3.58
P2	0.75:0.25	0.71:0.29	30.2	2.2	1.85	−5.45	−3.60
P3	0.50:0.50	0.41:0.59	31.1	2.7	1.86	−5.48	−3.62
P4	0.25:0.75	0.24:0.76	31.2	2.7	1.87	−5.49	−3.62
P5	0:1	0:1	25.9	2.3	1.88	−5.54	−3.66

[a]Values were determined by elemental analysis. [b]Values were determined by GPC. [c]Values were determined by UV−vis absorption spectra of thin films. [d]Values were determined by UPS. [e]Values were determined by LUMO = HOMO + E_g^{opt}.

overlapping π-orbitals that reduce the binding energy barrier of the excitons.[24,34−37] However, achieving such alignment between P_D and P_As at the interface during solvent-assisted formation of the active layer is nontrivial, hence leading to severe geminate charge recombination in all-PSCs. It is indeed one of the most dominant loss mechanisms in all-PSCs, though this has been less of a concern in fullerene-PSCs. Therefore, to guide further improvements in the performance of all-PSCs, specific focus should be placed on developing design rules for controlling the interfacial orientation of P_D and P_As in all-PSCs.

One insight into the design rules for all-PSCs was gained from our previous studies and those of others: the vast majority of high-performance all-PSCs used polymer donors appending 2D conjugated side chains (i.e., thienyl or phenyl groups).[3,4,6−9,34,36,38] These P_Ds typically surpass the performance of all-PSCs based on P_Ds with alkoxy side chains, even though both polymers with alkoxy- and 2D conjugated-side chains have been used extensively to produce high PCEs in fullerene-PSCs. For example, in our earlier work, all-PSCs based on the PTB7-Th with alkylthienyl side chains (PCE = 4.60%) outperformed those based on the PTB7 with alkoxy side chains (PCE = 2.54%),[33] while high PCEs of ∼10% were achieved in both PTB7 and PTB7-Th based fullerene-PSCs.[39,40] Hou and co-workers reported that the efficiency of PBDTBDD-T:PNDI all-PSCs having a P_D with conjugated alkylthienyl side chain (5.8%) was twice as high as compared to that of PBDTBDD:PNDI all-PSCs with a P_D having alkoxy side chain (2.4%).[34] These observations have two implications: (i) there exists different efficiency-determining principles between fullerene- and all-PSCs that are most likely linked to different morphological aspects in the active layers (e.g., interfacial orientation, as discussed above), and (ii) morphological aspects of all-PSCs can be modulated by engineering the side chains of conjugated polymers. It is expected that efforts to develop correlations between side chain structure, morphology, and device performance for all-PSCs will establish material design criteria for high-performance all-PSCs; however, very few studies have addressed these issues to date.[34,36]

Here we demonstrate the important role of 2D alkylthienyl conjugated side chains of polymer donors in manipulating the polymer packing, ordering and orientation relative to the P_D/P_A interface as well as the polymer composition variation in the BHJ domains. To systematically investigate the impact of side chains having 2D conjugation on the performance of all-PSC devices, we synthesized a series of poly(benzo[1,2-*b*:4,5-*b*̀]-dithiophene-thieno[3,4-*c*]pyrrole-4,6-dione (PBDTTPD) polymer donors containing different compositions of alkoxy and alkylthienyl side chains appended to the BDT backbone (Figure 1). We selected the PBDTTPD polymer backbone as a model system because PBDTTPD with both alkoxy and 2D conjugated alkylthienyl side chains produced similar, high PCEs (6−7%) with comparable short-circuit current density (J_{SC}) values in fullerene-based PSCs.[41−43] Increasing the fraction of alkylthienyl side chains in the polymer donors from 0 to 100 mol % enhanced the photovoltaic performances of naphthalenediimide-thiophene polymer acceptor (P(NDI2HD-T)) based all-PSCs from 2.82 to 6.60%. The significantly improved J_{SC} and fill factor (FF) values are attributed to enhanced charge transport and generation in the active layers and are the main contributors to the improved PCEs of all-PSCs. From grazing incidence X-ray scattering (GIXS) and resonant soft X-ray scattering (RSoXS) experiments, increasing trends in the population of face-on orientated polymers in the thin film blends, localized molecular orientation and ordering relative to the P_D/P_A interface, and composition variations (i.e., the average purity of the polymer domains) in the BHJ active layer were observed with increasing content of alkylthienyl side chains in the polymer donors.

DOI: 10.1021/acs.chemmater.7b03495
Chem. Mater. 2017, 29, 9407−9415

RESULTS AND DISCUSSION

A series of PBDTTPD polymer donors with different contents of alkoxy and alkylthienyl side chains was designed to investigate the effects of 2D conjugated side chains on the photovoltaic performance of all-PSCs (Figure 1). The side chain composition of the polymers was adjusted by varying the feed ratios of the 4,8-bis((2-ethylhexyloxy)benzo[1,2-b:4,5-b′]dithiophene-2,6-diyl)bis(trimethyl stannane) (BDT) and 4,8-bis(5-(2-ethylhexyl)thiophen-2-yl)benzo[1,2-b:4,5-b′]-dithiophene-2,6-diyl)bis(trimethyl stannane) (BDTT) monomers from 0 to 100 mol %, which produced five polymer donors: PBDT-TPD (**P1**, 0% BDTT), $PBDTT_{0.29}$-TPD (**P2**, 29% BDTT), $PBDTT_{0.59}$-TPD (**P3**, 59% BDTT), $PBDTT_{0.76}$-TPD (**P4**, 76% BDTT), and PBDTT-TPD (**P5**, 100% BDTT) (Figure S1). The BDT:BDTT ratios incorporated into the polymers were determined by elemental analysis, and the results showed good correlation with the molar feed ratios of BDT/BDTT monomers (Table 1). Detailed synthetic procedures are provided in the Supporting Information. The number-average molecular weight (M_n) and dispersity ($Đ$) of **P1**−**P5** were measured by gel permeation chromatography (GPC) (Table 1), and they exhibited similar M_n values (25.9−31.2 kg/mol). P(NDI2HD-T) polymer acceptor was synthesized following the previously reported procedure,[26] and the M_n and $Đ$ values of P(NDI2HD-T) were 65 kg/mol and 2.2, respectively. Ultraviolet photoelectron spectroscopy (UPS) was used to measure the highest occupied molecular orbital (HOMO) energy levels of **P1**−**P5** (Table 1, Figure S2). The HOMO energy levels of the polymers were determined to be −5.44 eV for **P1**, −5.45 eV for **P2**, −5.48 eV for **P3**, −5.49 eV for **P4**, and −5.54 eV for **P5**. The lowest occupied molecular orbital (LUMO) energy levels were estimated from the optical bandgaps (E^{opt}), and the LUMO levels of polymers were −3.58 eV for **P1**, −3.60 eV for **P2**, −3.62 eV for **P3**, −3.62 eV for **P4**, and −3.66 eV for **P5**. Both the HOMO and LUMO levels were found to decrease as the BDTT content in the P_Ds increased, which is likely because the π-electrons can be effectively delocalized along the extended π-conjugation of the BDTT units.[44,45] The gradually decreasing HOMO levels from **P1** to **P5** are beneficial for yielding higher open-circuit voltage (V_{OC}) values in all-PSC devices.

The optical properties of thin films of **P1**−**P5** were compared in Figure S3. All of the polymers exhibited broad and strong absorption bands in the range of 300−700 nm with similar maximum absorption coefficients in the range of (4.3−5.2) × 10^4 cm^{-1}. The intensity of the absorption peak at 615 nm was found to increase slightly with increasing amounts of alkylthienyl units in **P1** to **P5**, attributed mainly to the enhanced intermolecular $\pi-\pi$ interactions of the 2D conjugated alkylthienyl side chains of BDTT (Figure S3b).[45] However, the overall light absorption properties of the polymers remain relatively constant as a function of BDTT content. The absorption edges were essentially unchanged as a function of side chain composition, producing similar optical band gaps of 1.85−1.88 eV.

To evaluate the performance of **P1**−**P5**-based all-PSCs, we fabricated normal-type solar devices with an ITO/PEDOT:PSS/active layer/LiF/Al architecture. P(NDI2HD-T) was chosen as the P_A because of its good compatibility and high photovoltaic performance with PBDTT-TPD P_D.[3] For **P1**−**P5**-based all-PSCs, the optimal P_D/P_A ratio and active layer thickness were determined to be 1.3:1 (w/w) and 100−110 nm, respectively. The polymer blends were dissolved in chloroform, and 1 vol % 1, 8-diiodooctane (DIO) was added to the blend solutions to optimize the BHJ morphology. Device fabrication is detailed in the Supporting Information. The device performance of the all-PSCs is summarized in Table 2,

Table 2. Photovoltaic Performance of P1−P5:P(NDI2HD-T) All-PSCs

P_D	V_{OC} (V)	J_{SC} (mA cm^{-2})	FF	PCE_{max} (PCE_{avg}[a]) (%)	calculated J_{SC} (mA cm^{-2})
P1	0.96	7.35	0.40	2.82 (2.74)	7.13
P2	0.96	7.65	0.43	3.16 (3.08)	7.41
P3	0.99	8.73	0.51	4.41 (4.31)	8.41
P4	1.00	10.43	0.51	5.32 (5.28)	10.10
P5	1.04	11.13	0.57	6.60 (6.32)	10.60

[a]Average PCEs obtained from at least 10 devices are shown in parentheses.

and the current density−voltage ($J-V$) and the external quantum efficiency (EQE) curves are displayed in Figure 2. Interestingly, we found that there was a linear trend between PCE and BDTT content in the P_Ds : PCEs were increased from 2.82% for **P1**, 3.16% for **P2**, 4.41% for **P3**, 5.32% for **P4**, and 6.60% for **P5**. The V_{oc} increased from 0.96 (**P1**) to 0.99 (**P3**), and to 1.04 (**P5**), as a result of the decreased HOMO levels of the polymers as a function of BDTT content. However, we noted that the simultaneously increased *Jsc* and FF values were the dominant factors responsible for the strong correlation between the side chain composition of the P_D s and the PCEs. For example, the **P1** device afforded low *Jsc* and FF values of 7.35 mA/cm^2 and 0.40, respectively, whereas the **P5** device yielded much higher values of 11.13 mA/cm^2 and 0.57, which were 51% and 43% increases, respectively. The EQE spectra of the **P1**−**P5** devices supported the increasing *Jsc* values with BDTT content in the P_Ds (Figure 2b). While all of the devices yielded broad EQE responses from 300 to 700 nm, the EQE values progressively increased in the order of **P1**, **P2**, **P3**, **P4**, and **P5**-based all-PSCs. The integrated *Jsc* values from the EQE spectra correlated well with the *Jsc* values measured from the solar cell devices, within 5% error.

It is worth noting that the PCE trends of all-PSCs differed greatly from those of fullerene-PSCs constructed with the same P_Ds (i.e., **P1** and **P5**). We fabricated **P1**- and **P5**-based fullerene-PSCs following conditions in the literature.[41−43] The PCEs of both **P1**- and **P5**-based fullerene-PSCs were not sensitive to side chain structure, yielding similar PCEs of ∼6% and comparable *Jsc* values of ∼12 mA cm^{-2} (Table S1). Additionally, previous work by Beaujuge et al. supported our observations. They reported the PCE of PBDT-TPD (**P1**)-based fullerene-PSCs to be 7.5%, which exceeded that of the fullerene-PSC fabricated with PBDTT-TPD having 2D side chains (6.5%).[41,42] Taken together with the photovoltaic performance of the **P1**−**P5**-based all-PSCs reported herein, this report suggests that the drastic contrast in the photovoltaic performances of the **P1**−**P5** all-PSCs originated from different underlying working principles in all-PSCs and fullerene-PSCs. Further, since the light absorption properties of the **P1**−**P5**-based all-PSCs were similar (Figure S4), it was expected that the electrical properties (i.e., charge transport and exciton dissociation) of the BHJ active layers would be the dominant factor in determining the photovoltaic performance.

DOI: 10.1021/acs.chemmater.7b03495
Chem. Mater. 2017, 29, 9407−9415

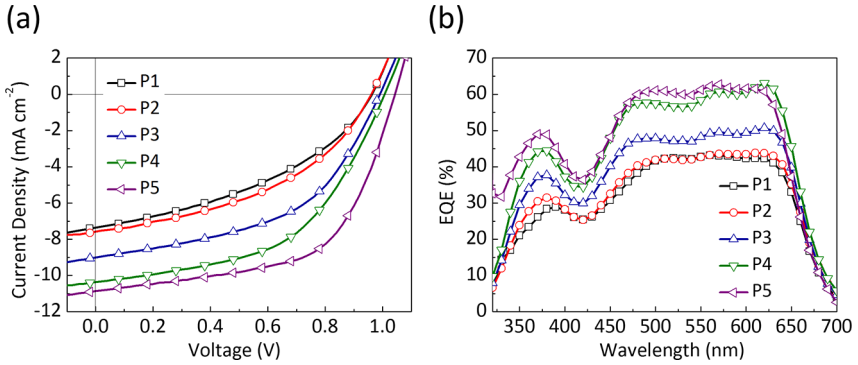

Figure 2. (a) $J-V$ curves and (b) EQE responses of **P1**−**P5**:P(NDI2HD-T) all-PSCs.

To evaluate the charge transport properties of **P1**−**P5** all-PSCs, the hole (μ_h) and electron (μ_e) mobilities were measured using the space-charge limited current (SCLC) method (Table S2). We found an increasing trend in the average μ_h as a function of BDTT content, from 5.42×10^{-6} cm^2 V^{-1} s^{-1} for **P1**, to 6.35×10^{-6} cm^2 V^{-1} s^{-1} for **P2**, to 7.98×10^{-6} cm^2 V^{-1} s^{-1} for **P3**, to 1.43×10^{-5} cm^2 V^{-1} s^{-1} for **P4**, and to 4.41×10^{-5} cm^2 V^{-1} s^{-1} for **P5**. However, the μ_e values of the **P1**−**P5**:P(NDI2HD-T) blend films were almost constant, that is, $(5.05-6.45) \times 10^{-5}$ cm^2 V^{-1} s^{-1}. As such, the **P5**:P(NDI2HD-T) blend afforded well-balanced electron and hole mobilities (μ_e/μ_h = 1.26). Next, the exciton dissociation probability ($P(E,T)$) of the **P1**−**P5**:P(NDI2HD-T)-based all-PSCs was investigated to gauge the geminate recombination losses in the devices. The photocurrent densities (J_{ph}) of the devices were measured against biased voltages between −6 and +2 V under illumination (100 mW cm^{-2}) and in the dark, and the J_{ph} versus effective voltage (V_{eff}) curves were plotted (Figure 3), where J_{ph}

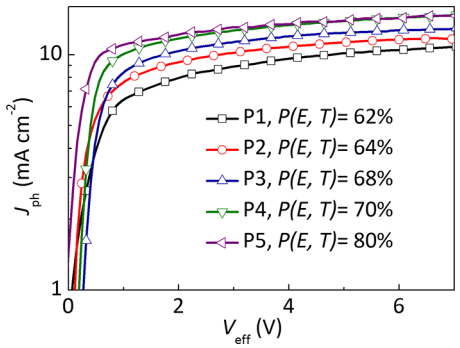

Figure 3. Photocurrent density (J_{ph}) versus effective voltage (V_{eff}) of **P1**−**P5** all-PSCs.

and V_{eff} are defined as $J_{illumination} - J_{dark}$ and $V_0 - V_{applied}$, respectively (V_0 is the voltage when J_{ph} = 0, and $V_{applied}$ is the applied bias). The $P(E,T)$ values were obtained by calculating the ratio of J_{ph} at the short circuit condition ($V_{eff} = V_0$) and the saturated photocurrent density $J_{ph,sat}$.[46−49] $P(E,T)$ values for the **P1**−**P5** devices were calculated to be 62, 64, 68, 70 and 80%, respectively. Taken together, the increased exciton dissociation and improved charge transport as a function of the incorporation of BDTT contributed to the enhancement in Jsc and FF, and thus the resulting PCEs in **P5** all-PSCs.

Charge transport and exciton dissociation in all-PSCs are strongly correlated with structural and morphological characteristics. To investigate the polymer packing structure, orientation, and blend morphology in **P1**−**P5** all-PSCs, complementary analyses using GIXS, RSoXS, atomic force microscopy (AFM), and photoluminescence (PL) spectroscopy were performed. First, GIXS was used to investigate the molecular packing and the crystallinity of **P1**−**P5** in both neat polymer films and their blends with the P(NDI2HD-T) polymer acceptor. We prepared **P1**−**P5** thin films on Si/PEDOT:PSS substrates by spin-coating from chloroform. Figure S5 displays the 2D GIXS patterns of **P1**−**P5** films and their line cuts in the in-plane and out-of-plane directions. All of the polymers were found to exhibit clear (100) reflection peaks in the in-plane direction with lamellar spacings ($d_{100,in}$) of 2.14 nm (**P1**), 2.25 nm (**P2**), 2.29 nm (**P3**), 2.33 nm (**P4**), and 2.39 nm (**P5**) (Table 3). The lamellar spacings gradually increased due to increased amounts of extended 2D side chains in the BDTT units. We compared the coherence length (L_c) of the crystalline domains of **P1**−**P5** measured from the in-plane (100) lamellar stacking peaks using the Scherrer equation (Table 3).[50−52] A monotonic increase in L_c values was observed as a function of BDTT content, from 8.5 nm (**P1**), to 9.7 nm (**P3**), and 11.3 nm (**P5**). This result suggests that the 2D conjugated alkylthienyl side chains are beneficial in that they induce the formation of larger crystallites in thin films. Importantly, we observed significant differences in the packing orientation of the polymer crystallites between **P1**−**P5** films. The **P1** film produced distinct (010) $\pi-\pi$

Table 3. Morphological Characteristics of P1−P5 Pristine and Blend Films

P_D	$d_{100,in}$[a] (nm)	$d_{010,out}$[a] (nm)	$L_{c100,in}$[a] (nm)	F/E ratio[a]	domain spacing[b] (nm)	anisotropy parameter[b]	relative domain purity[b]
P1	2.14	0.365	8.5	2.2	42.8	0	0.19
P2	2.25	0.367	9.1		47.9		0.63
P3	2.29	0.370	9.7	5.3	43.9	−0.15	0.74
P4	2.33	0.372	11.0		55.7		0.74
P5	2.39	0.376	11.3	10.1	52.4	−0.31	1

[a]Values associated with pristine films. [b]Values associated with blend films. Relative face-on/edge-on ratio (F/E) was derived from the (010) peak area of **P1**−**P5** in the range of χ = 0−45° and χ = 45−90°.

DOI: 10.1021/acs.chemmater.7b03495
Chem. Mater. 2017, 29, 9407−9415

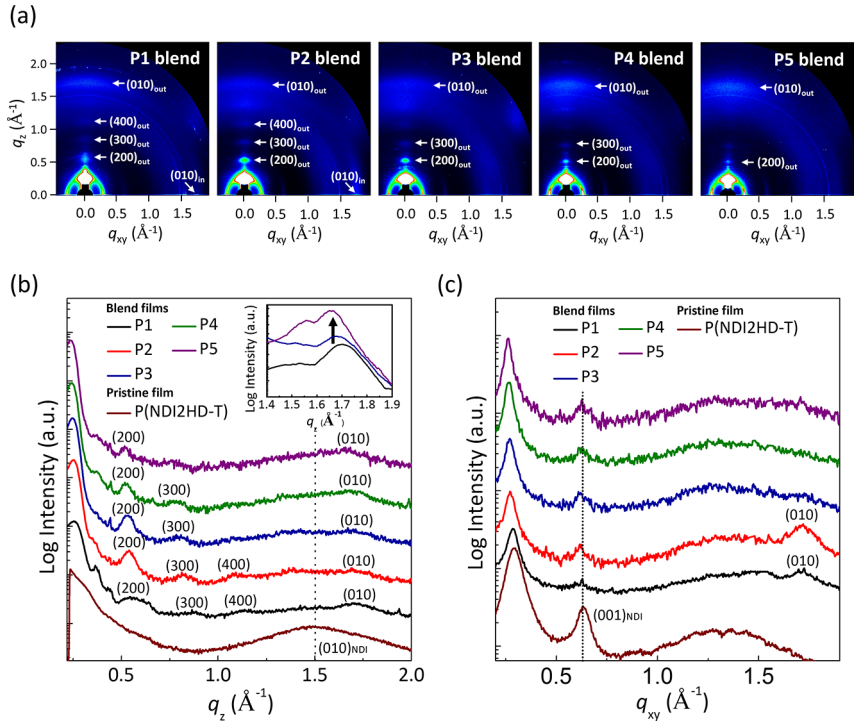

Figure 4. (a) 2D GIXS patterns of **P1**−**P5**:P(NDI2HD-T) all-PSCs and their line cuts in the (b) out-of-plane and (c) in-plane directions.

stacking reflection peaks in both the in-plane and out-of-plane directions, indicating that both edge-on and face-on orientations of **P1** crystallites were present in the thin film. With increasing BDTT content, the (010) peak in the in-plane direction began to disappear, and, simultaneously, the (010) peak in the out-of-plane direction became stronger. Therefore, the **P5** polymer film contained mostly face-on oriented crystallites. High-order peaks of lamellar stacking up to (300) were observed in **P1** thin films, and these peaks decreased monotonically with increasing BDTT content, which confirmed the sequential changes observed in the molecular orientation as a function of BDTT content.

On the basis of the understanding of the para-crystalline behaviors of **P1**−**P5**, we investigated the polymer packing structures in **P1**−**P5**:P(NDI2HD-T) blend films by GIXS (Figure 4). All samples were prepared under identical conditions used to fabricate optimized devices. Consistent with the observations in the pristine thin films, higher order (h00) lamellar reflection peaks up to (400) in the out-of-plane direction (q_z) and pronounced (010) π−π stacking peaks in the in-plane direction (q_{xy}) were seen in the polymer donors with low BDTT contents (e.g., **P1** and **P2**). However, as the BDTT content increased, both peaks faded and a monotonic increase in the intensity of the (010) π−π stacking peaks was observed in the q_z direction (inset of Figure 4b). This indicated that the intrinsic molecular orientation of **P1**−**P5** was preserved in the blend films with the P(NDI2HD-T) polymer acceptor. The P(NDI2HD-T) P_A also exhibited strong face-on packing in thin films (Figure S6),[3,26] and the (001) peak in the q_{xy} direction associated with the P(NDI2HD-T) backbone was preserved in the blend films (Figure 4c). Consequently, it is postulated that the **P5** donor with strong face-on orientation likely produced well-defined, face-to-face alignment with P(NDI2HD-T) acceptor at the P_D/P_A interfaces, whereas the **P1** donor with mixed orientations led to the misoriented P_D/P_A interfaces.

To quantify the differences in the molecular orientation of **P1**−**P5** in thin films, the pole figures for each of the polymers were obtained (Figure 5). The GIXS patterns for **P1**, **P3**, and

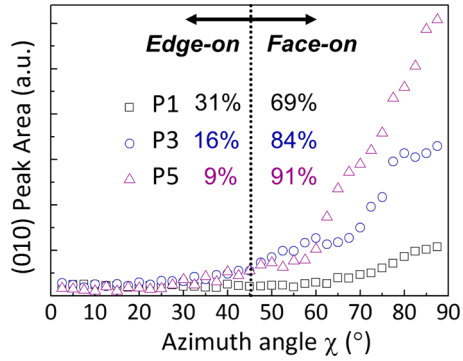

Figure 5. Pole figures from the (010) peak area of **P1**, **P3** and **P5** films; the fractions correspond to the relative ratios of integrated 0−45° and 45−90° peaks to the summed area.

P5 pristine films were used to elucidate the quantitative differences between polymer orientation in thin films. The pole figure was obtained as follows. First, the (010) π−π stacking peak intensities of **P1**, **P3**, and **P5** as a function of azimuth angles (χ, 0−90°) were extracted from the line cut data along the radial direction every 2.5°.[24,50] Then the area of each (010) crystalline peak (per cutting line) was plotted as a function of azimuth angle measured every 2.5° to produce the pole figure, where χ is an angle with respect to the q_{xy} axis, that is, χ = 0° is the in-plane axis (q_{xy}) and χ = 90° is the out-of-plane axis (q_z). Thus, the relative face-on/edge-on ratio (F/E) was derived from the (010) peak area in the range of χ = 45−90° and χ = 0−45°. As shown in Figure 5, a contrast in the face-on/edge-on distribution between the **P1**, **P3**, and **P5** films was observed. A mixture of face-on and edge-on packing was observed in the **P1**

DOI: 10.1021/acs.chemmater.7b03495
Chem. Mater. 2017, 29, 9407−9415

thin films in portions of 69 and 31%, respectively, resulting in an F/E ratio of 2.2. Upon incorpration of BDTT monomers with 2D side chain, the primarily edge-on orientation was transformed gradually to a face-on orientation. Thin films of **P5** had the highest face-on population of 91%, corresponding to an F/E ratio of 10.1. The high population of face-on structures can promote vertical charge transport in all-PSCs.[53−55] In addition, this feature of **P5** film is anticipated to promote the formation of face-to-face alignment of the P_D and P_A at the interface and facilitate efficient exciton dissociation.

To gain deeper insight into the impact of 2D side chains on the interfacial orientation of polymers in all-PSCs, transmission RSoXS experiments were performed at different photon energies. RSoXS with a polarized soft X-ray beam allows probing of the in-plane, localized molecular orientation and ordering of the components relative to the P_D/P_A interface through analysis of scattering anisotropy.[11,34,56−58] First, we prepared **P1**, **P3**, **P5**, and P(NDI2HD-T) pristine films and acquired near edge X-ray absorption fine structure (NEXAFS) profiles to assign bond transition energies of the polymers (Figure S7). All of the polymers exhibited a strong bond transition at a photon energy of 287.5 eV, which is commonly associated with combined contributions of carbon−hydrogen or carbon−sulfur 1s-$\sigma^*_{C-H\ or\ C-S}$ bond transitions.[59] The pronounced peaks at 285.4 eV photon energy were also observed in the **P1**, **P3**, and **P5** films, which are related to the 1s-$\pi^*_{C=C}$ bond transitions of the conjugated polymer backbone. Since the P(NDI2HD-T) P_A film did not show a distinct bond transition at 285.4 eV, we selected a photon energy of 285.4 eV to compare the peak characteristics of **P1**, **P3**, and **P5** in blend films without interference from P_A (Figure S8). When we applied a horizontally polarized soft X-ray beam to the samples, distinct contrast between the scattering anisotropy was observed between the three blends. The scattering ring in the **P1** blend film was nearly isotropic, but the anisotropy increased in **P3** films, and more so in the **P5** blend films. Therefore, the **P5** blend film exhibited the most anisotropic pattern with stronger scattering intensity in the horizontal direction. Next, we attempted to obtain quantitative differences in the scattering anisotropy of the three blend films using the integrated scattering intensity (ISI) and the following equation,[58] $(ISI_{\perp}-ISI_{\parallel})/(ISI_{\perp}+ISI_{\parallel})$ (a phenomenological anisotropy parameter). $ISI_{\perp}$ and $ISI_{\parallel}$ were calculated from the average sector line cuts (±10°) of the 2D scattering patterns in the perpendicular and parallel directions, respectively (Figure S9, Table 3). The anisotropy ranged from 0 for the **P1** blend, to −0.15 for the **P3** blend, and −0.31 for the **P5** blend. The magnitude of the anisotropy can be changed only when the 1s-$\pi^*_{C=C}$ transition dipole moments from the polymeric backbones are highly aligned (either horizontally or perpendicularly) with the applied electrical field direction. Therefore, this feature indicates the greatly increased extent of molecular orientational order of **P5** chains relative to the P_D/P_A interface. In contrast, the isotropic 2D scattering pattern of the **P1** film suggests the presence of randomly oriented **P1** chains relative to the P_D/P_A interface. Additional polarized RSoXS results for the **P1**, **P3**, **P5**, and P(NDI2HD-T) pristine films provided further evidence concerning this observation (Figure S10). In stark contrast to the scattering patterns of the blend films, the **P1**, **P3**, **P5**, and P(NDI2HD-T) pristine films showed nearly isotropic scattering patterns. Therefore, it was concluded that high scattering anisotropy of the **P5** blend film was the result of molecular anisotropy ralative to the P_D/P_A interface, attributed to $\pi-\pi$ stacking of **P5** with the blended P(NDI2HD-T) near the interface and/or additional aggregation of **P5** in the blend film.[34,57] The correlated π-orbitals of **P5** and P(NDI2HD-T) at the P_D/P_A interface are expected to improve exciton dissociation at the interface, which correlates well with the $P(E,T)$ and Jsc values in the all-PSCs.[34−36,60] However, extensive interpretation of the chain orientation behaviors, which can be only achieved by appropriate X-ray optical models that require anisotropic optical constants for **P1**, **P3**, **P5**, and P(NDI2HD-T), is beyond the scope of this paper. Recently, Ye et al. thoroughly described the impact of interfacial orientation of the polymer donor (PBDTBDD-T) on the performance of all-PSCs using polarized RSoXS measurements and optical models.[34] They observed strong anisotropic patterns in the PBDTBDD-T:NDI-based P_A blends with a high anisotropy ratio of −0.45, indicating the face-on alignment of PBDTBDD-T polymers with respect to the P_D/P_A interface. This conclusion is consistent with our observations in this work.

Next we investigated additional morphological characteristics (i.e., the domain spacing and purity) of **P1**−**P5** all-polymer blends using RSoXS at a different photon energy, namely 287.5 eV. At this energy, the material contrast of the blend films was maximized with marginal contribution from mass−thickness differences. Five **P1**−**P5** blend samples were prepared under the optimized device fabrication conditions. RSoXS profiles were plotted as a function of scattering vector q (nm^{-1}) in Figure 6. All of the samples exhibited broad scattering peaks in the range of q = 0.05−0.3 nm^{-1} and the peaks were centered at similar q_{peak} values of 0.11−0.15 nm^{-1}. Therefore, the **P1**−**P5** blend films exhibited finely phase-separated BHJ morphologies with similar domain spacings ($d = 2\pi/q_{peak}$) of 43−56 nm (Table 3), which was well-supported by AFM measurements (Figure S11). Also, all of the blend films produced similar PL quenching, suggesting similar domain spacings of the BHJ morphologies of **P1**−**P5** blend films (Figure S12). However, singificant differences in the scattering intensities of the **P1**−**P5** blend films were observed. The intensities progressively increased from **P1** to **P5** blends, indicating a higher purity of P_D and P_A domains in blends with P_Ds having higher BDTT contents. The relative root−mean−square composition variation, related to domain purity, is proportional to $\sqrt{ISI}$ (Table 3).[61−64] The relative $\sqrt{ISI}$ increased significantly from 0.19 in the **P1** blend to 0.74 in the **P3** blend, and 1 in the **P5** blend, which was used a reference. Thus, the root-mean square composition variations of the **P5** blend was determined to be 5.3 times greater than that of the **P1** blend. The underlying increased domain purity is attributed to the improved

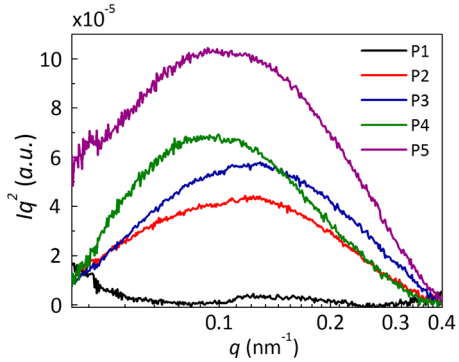

Figure 6. RSoXS profiles of **P1**−**P5** blend films.

DOI: 10.1021/acs.chemmater.7b03495
Chem. Mater. 2017, 29, 9407−9415

molecular packing of the **P5** polymer,[62,65] which is in good agreement with UV−vis and GIXS results. The relatively pure domains with finely phase-separated BHJ morphologies of **P5** blends yielded improved charge transport and efficient exciton dissociation in all-PSCs.

CONCLUSIONS

In this work, we demonstrated the importance of 2D conjugated side chains (BDTT) for producing efficient all-PSCs based on the model polymer donors, **P1**−**P5**. We observed a strong correlation of the BDTT content in the polymer donors with the *J*sc and FF values and the resulting photovoltaic performances of the all-PSCs. The increase in BDTT content generated gradual enhancement in the PCEs of all-PSCs from 2.82% (**P1**), to 3.16% (**P2**), to 4.41% (**P3**), to 5.32% (**P4**), and to 6.60% (**P5**). From the structural and morphological investigation using GIXS and RSoXS measurements, it was concluded that the use of the π-extended BDTT units enhanced the face-on crystalline domains of P_D in thin films and promoted strong $\pi-\pi$ interactions with P_A. These features impacted both the interfacial ordering of the P_Ds and P_A and the relative domain purity in the active blend layer. For example, the **P5**-based all-polymer blends exhibited the highest coherence length of face-on crystalline domains and the highest domain purity. The dramatic changes in morphological characteristics with side chain composition improved hole mobility and $P(E,T)$ of **P5**-based all-PSCs, leading to greatly enhanced *J*sc and FF values. The structure−property-performance correlations established in our model system provide important guidelines for designing effective P_D and P_A polymers in terms of the side chain structure and demonstrate the importance of controlling the polymer orientation and domain purity to achieve high-performance all-PSCs.

ASSOCIATED CONTENT

Supporting Information

The Supporting Information is available free of charge on the ACS Publications website at DOI: 10.1021/acs.chemmater.7b03495.

Materials and methods, detailed experimental procedures, additional data (PDF)

AUTHOR INFORMATION

Corresponding Author

*E-mail: bumjoonkim@kaist.ac.kr.

ORCID

Bumjoon J. Kim: 0000-0001-7783-9689

Notes

The authors declare no competing financial interest.

ACKNOWLEDGMENTS

This research was supported by the National Research Foundation Grant (2012M3A6A7055540, 2015M1A2A2057509), funded by the Korean Government. We acknowledge additional support for this work from the Research Projects of the KAIST-KUSTAR. H.A. was supported by NSF INFEWS Grant No. CBET 1639429. We thank Dr. Rachel Letteri for the helpful discussions. We acknowledge Nam Young Ahn and Prof. Myungeun Seo for the assistance in the GPC measurements.

REFERENCES

(1) Benten, H.; Mori, D.; Ohkita, H.; Ito, S. Recent research progress of polymer donor/polymer acceptor blend solar cells. *J. Mater. Chem. A* **2016**, *4*, 5340−5365.

(2) Kang, H.; Lee, W.; Oh, J.; Kim, T.; Lee, C.; Kim, B. J. From Fullerene−Polymer to All-Polymer Solar Cells: The Importance of Molecular Packing, Orientation, and Morphology Control. *Acc. Chem. Res.* **2016**, *49*, 2424−2434.

(3) Kim, T.; Kim, J.-H.; Kang, T. E.; Lee, C.; Kang, H.; Shin, M.; Wang, C.; Ma, B.; Jeong, U.; Kim, T.-S.; Kim, B. J. Flexible, highly efficient all-polymer solar cells. *Nat. Commun.* **2015**, *6*, 8547.

(4) Fan, B.; Ying, L.; Wang, Z.; He, B.; Jiang, X.-F.; Huang, F.; Cao, Y. Optimisation of processing solvent and molecular weight for the production of green-solvent-processed all-polymer solar cells with a power conversion efficiency over 9%. *Energy Environ. Sci.* **2017**, *10*, 1243−1251.

(5) Li, Z.; Zhang, W.; Xu, X.; Genene, Z.; Di Carlo Rasi, D.; Mammo, W.; Yartsev, A.; Andersson, M. R.; Janssen, R. A. J.; Wang, E. High-Performance and Stable All-Polymer Solar Cells Using Donor and Acceptor Polymers with Complementary Absorption. *Adv. Energy Mater.* **2017**, *7*, 1602722.

(6) Gao, L.; Zhang, Z.-G.; Xue, L.; Min, J.; Zhang, J.; Wei, Z.; Li, Y. All-Polymer Solar Cells Based on Absorption-Complementary Polymer Donor and Acceptor with High Power Conversion Efficiency of 8.27%. *Adv. Mater.* **2016**, *28*, 1884−1890.

(7) Hwang, Y.-J.; Courtright, B. A. E.; Ferreira, A. S.; Tolbert, S. H.; Jenekhe, S. A. 7.7% Efficient All-Polymer Solar Cells. *Adv. Mater.* **2015**, *27*, 4578−4584.

(8) Chen, S.; An, Y.; Dutta, G. K.; Kim, Y.; Zhang, Z.-G.; Li, Y.; Yang, C. A Synergetic Effect of Molecular Weight and Fluorine in All-Polymer Solar Cells with Enhanced Performance. *Adv. Funct. Mater.* **2017**, *27*, 1603564.

(9) Oh, J.; Kranthiraja, K.; Lee, C.; Gunasekar, K.; Kim, S.; Ma, B.; Kim, B. J.; Jin, S.-H. Side-Chain Fluorination: An Effective Approach to Achieving High-Performance All-Polymer Solar Cells with Efficiency Exceeding 7%. *Adv. Mater.* **2016**, *28*, 10016−10023.

(10) Jung, J. W.; Jo, J. W.; Chueh, C.-C.; Liu, F.; Jo, W. H.; Russell, T. P.; Jen, A. K. Y. Fluoro-Substituted n-Type Conjugated Polymers for Additive-Free All-Polymer Bulk Heterojunction Solar Cells with High Power Conversion Efficiency of 6.71%. *Adv. Mater.* **2015**, *27*, 3310−3317.

(11) Ye, L.; Jiao, X.; Zhao, W.; Zhang, S.; Yao, H.; Li, S.; Ade, H.; Hou, J. Manipulation of Domain Purity and Orientational Ordering in High Performance All-Polymer Solar Cells. *Chem. Mater.* **2016**, *28*, 6178−6185.

(12) Li, S.; Zhang, H.; Zhao, W.; Ye, L.; Yao, H.; Yang, B.; Zhang, S.; Hou, J. Green-Solvent-Processed All-Polymer Solar Cells Containing a Perylene Diimide-Based Acceptor with an Efficiency over 6.5%. *Adv. Energy Mater.* **2016**, *6*, 1501991.

(13) Long, X.; Ding, Z.; Dou, C.; Zhang, J.; Liu, J.; Wang, L. Polymer Acceptor Based on Double B←N Bridged Bipyridine (BNBP) Unit for High-Efficiency All-Polymer Solar Cells. *Adv. Mater.* **2016**, *28*, 6504−6508.

(14) Zhao, R.; Dou, C.; Xie, Z.; Liu, J.; Wang, L. Polymer Acceptor Based on B←N Units with Enhanced Electron Mobility for Efficient All-Polymer Solar Cells. *Angew. Chem., Int. Ed.* **2016**, *55*, 5313−5317.

(15) Benten, H.; Nishida, T.; Mori, D.; Xu, H.; Ohkita, H.; Ito, S. High-performance ternary blend all-polymer solar cells with complementary absorption bands from visible to near-infrared wavelengths. *Energy Environ. Sci.* **2016**, *9*, 135−140.

(16) Guo, Y.; Li, Y.; Awartani, O.; Zhao, J.; Han, H.; Ade, H.; Zhao, D.; Yan, H. A Vinylene-Bridged Perylenediimide-Based Polymeric Acceptor Enabling Efficient All-Polymer Solar Cells Processed under Ambient Conditions. *Adv. Mater.* **2016**, *28*, 8483−8489.

(17) Guo, Y.; Li, Y.; Awartani, O.; Han, H.; Zhao, J.; Ade, H.; Yan, H.; Zhao, D. Improved Performance of All-Polymer Solar Cells Enabled by Naphthodiperylenetetraimide-Based Polymer Acceptor. *Adv. Mater.* **2017**, *29*, 1700309.

DOI: 10.1021/acs.chemmater.7b03495
Chem. Mater. 2017, 29, 9407−9415

(18) Li, Z.; Xu, X.; Zhang, W.; Meng, X.; Ma, W.; Yartsev, A.; Inganäs, O.; Andersson, M. R.; Janssen, R. A. J.; Wang, E. High Performance All-Polymer Solar Cells by Synergistic Effects of Fine-Tuned Crystallinity and Solvent Annealing. *J. Am. Chem. Soc.* **2016**, *138*, 10935−10944.
(19) Liu, S.; Kan, Z.; Thomas, S.; Cruciani, F.; Brédas, J.-L.; Beaujuge, P. M. Thieno[3,4-c]pyrrole-4,6-dione-3,4-difluorothiophene Polymer Acceptors for Efficient All-Polymer Bulk Heterojunction Solar Cells. *Angew. Chem.* **2016**, *128*, 13190−13194.
(20) Hwang, Y.-J.; Earmme, T.; Courtright, B. A. E.; Eberle, F. N.; Jenekhe, S. A. n-Type Semiconducting Naphthalene Diimide-Perylene Diimide Copolymers: Controlling Crystallinity, Blend Morphology, and Compatibility Toward High-Performance All-Polymer Solar Cells. *J. Am. Chem. Soc.* **2015**, *137*, 4424−4434.
(21) Earmme, T.; Hwang, Y.-J.; Murari, N. M.; Subramaniyan, S.; Jenekhe, S. A. All-Polymer Solar Cells with 3.3% Efficiency Based on Naphthalene Diimide-Selenophene Copolymer Acceptor. *J. Am. Chem. Soc.* **2013**, *135*, 14960−14963.
(22) Li, Z.; Xu, X.; Zhang, W.; Meng, X.; Genene, Z.; Ma, W.; Mammo, W.; Yartsev, A.; Andersson, M. R.; Janssen, R. A. J.; Wang, E. 9.0% power conversion efficiency from ternary all-polymer solar cells. *Energy Environ. Sci.* **2017**, *10*, 2212.
(23) Kang, H.; Uddin, M. A.; Lee, C.; Kim, K.-H.; Nguyen, T. L.; Lee, W.; Li, Y.; Wang, C.; Woo, H. Y.; Kim, B. J. Determining the Role of Polymer Molecular Weight for High-Performance All-Polymer Solar Cells: Its Effect on Polymer Aggregation and Phase Separation. *J. Am. Chem. Soc.* **2015**, *137*, 2359−2365.
(24) Jung, J.; Lee, W.; Lee, C.; Ahn, H.; Kim, B. J. Controlling Molecular Orientation of Naphthalenediimide-Based Polymer Acceptors for High Performance All-Polymer Solar Cells. *Adv. Energy Mater.* **2016**, *6*, 1600504.
(25) Zhou, N.; Dudnik, A. S.; Li, T. I. N. G.; Manley, E. F.; Aldrich, T. J.; Guo, P.; Liao, H.-C.; Chen, Z.; Chen, L. X.; Chang, R. P. H.; Facchetti, A.; Olvera de la Cruz, M.; Marks, T. J. All-Polymer Solar Cell Performance Optimized via Systematic Molecular Weight Tuning of Both Donor and Acceptor Polymers. *J. Am. Chem. Soc.* **2016**, *138*, 1240−1251.
(26) Lee, C.; Kang, H.; Lee, W.; Kim, T.; Kim, K.-H.; Woo, H. Y.; Wang, C.; Kim, B. J. High-Performance All-Polymer Solar Cells Via Side-Chain Engineering of the Polymer Acceptor: The Importance of the Polymer Packing Structure and the Nanoscale Blend Morphology. *Adv. Mater.* **2015**, *27*, 2466−2471.
(27) Lee, W.; Lee, C.; Yu, H.; Kim, D.-J.; Wang, C.; Woo, H. Y.; Oh, J. H.; Kim, B. J. Side Chain Optimization of Naphthalenediimide−Bithiophene-Based Polymers to Enhance the Electron Mobility and the Performance in All-Polymer Solar Cells. *Adv. Funct. Mater.* **2016**, *26*, 1543−1553.
(28) Zhou, Y.; Kurosawa, T.; Ma, W.; Guo, Y.; Fang, L.; Vandewal, K.; Diao, Y.; Wang, C.; Yan, Q.; Reinspach, J.; Mei, J.; Appleton, A. L.; Koleilat, G. I.; Gao, Y.; Mannsfeld, S. C. B.; Salleo, A.; Ade, H.; Zhao, D.; Bao, Z. High Performance All-Polymer Solar Cell via Polymer Side-Chain Engineering. *Adv. Mater.* **2014**, *26*, 3767−3772.
(29) Cho, H.-H.; Kim, T.; Kim, K.; Lee, C.; Kim, F. S.; Kim, B. J. Synthesis and side-chain engineering of phenylnaphthalenediimide (PNDI)-based n-type polymers for efficient all-polymer solar cells. *J. Mater. Chem. A* **2017**, *5*, 5449−5459.
(30) Zhao, R.; Bi, Z.; Dou, C.; Ma, W.; Han, Y.; Liu, J.; Wang, L. Polymer Electron Acceptors with Conjugated Side Chains for Improved Photovoltaic Performance. *Macromolecules* **2017**, *50*, 3171−3178.
(31) Cho, C.-H.; Kim, H. J.; Kang, H.; Shin, T. J.; Kim, B. J. The effect of side-chain length on regioregular poly[3-(4-n-alkyl)-phenylthiophene]/PCBM and ICBA polymer solar cells. *J. Mater. Chem.* **2012**, *22*, 14236−14245.
(32) Hwang, Y.-J.; Earmme, T.; Subramaniyan, S.; Jenekhe, S. A. Side chain engineering of n-type conjugated polymer enhances photocurrent and efficiency of all-polymer solar cells. *Chem. Commun.* **2014**, *50*, 10801−10804.
(33) Kang, H.; Kim, K.-H.; Choi, J.; Lee, C.; Kim, B. J. High-Performance All-Polymer Solar Cells Based on Face-On Stacked Polymer Blends with Low Interfacial Tension. *ACS Macro Lett.* **2014**, *3*, 1009−1014.
(34) Ye, L.; Jiao, X.; Zhou, M.; Zhang, S.; Yao, H.; Zhao, W.; Xia, A.; Ade, H.; Hou, J. Manipulating Aggregation and Molecular Orientation in All-Polymer Photovoltaic Cells. *Adv. Mater.* **2015**, *27*, 6046−6054.
(35) Schubert, M.; Collins, B. A.; Mangold, H.; Howard, I. A.; Schindler, W.; Vandewal, K.; Roland, S.; Behrends, J.; Kraffert, F.; Steyrleuthner, R.; Chen, Z.; Fostiropoulos, K.; Bittl, R.; Salleo, A.; Facchetti, A.; Laquai, F.; Ade, H. W.; Neher, D. Correlated Donor/Acceptor Crystal Orientation Controls Photocurrent Generation in All-Polymer Solar Cells. *Adv. Funct. Mater.* **2014**, *24*, 4068−4081.
(36) Deshmukh, K. D.; Prasad, S. K. K.; Chandrasekaran, N.; Liu, A. C. Y.; Gann, E.; Thomsen, L.; Kabra, D.; Hodgkiss, J. M.; McNeill, C. R. Critical Role of Pendant Group Substitution on the Performance of Efficient All-Polymer Solar Cells. *Chem. Mater.* **2017**, *29*, 804−816.
(37) Zhou, K.; Zhang, R.; Liu, J.; Li, M.; Yu, X.; Xing, R.; Han, Y. Donor/Acceptor Molecular Orientation-Dependent Photovoltaic Performance in All-Polymer Solar Cells. *ACS Appl. Mater. Interfaces* **2015**, *7*, 25352−25361.
(38) Shi, S.; Yuan, J.; Ding, G.; Ford, M.; Lu, K.; Shi, G.; Sun, J.; Ling, X.; Li, Y.; Ma, W. Improved All-Polymer Solar Cell Performance by Using Matched Polymer Acceptor. *Adv. Funct. Mater.* **2016**, *26*, 5669−5678.
(39) He, Z.; Zhong, C.; Su, S.; Xu, M.; Wu, H.; Cao, Y. Enhanced power-conversion efficiency in polymer solar cells using an inverted device structure. *Nat. Photonics* **2012**, *6*, 591−595.
(40) He, Z.; Xiao, B.; Liu, F.; Wu, H.; Yang, Y.; Xiao, S.; Wang, C.; Russell, T. P.; Cao, Y. Single-junction polymer solar cells with high efficiency and photovoltage. *Nat. Photonics* **2015**, *9*, 174−179.
(41) Cabanetos, C.; El Labban, A.; Bartelt, J. A.; Douglas, J. D.; Mateker, W. R.; Fréchet, J. M. J.; McGehee, M. D.; Beaujuge, P. M. Linear Side Chains in Benzo[1,2-b:4,5-b′]dithiophene−Thieno[3,4-c]pyrrole-4,6-dione Polymers Direct Self-Assembly and Solar Cell Performance. *J. Am. Chem. Soc.* **2013**, *135*, 4656−4659.
(42) Warnan, J.; El Labban, A.; Cabanetos, C.; Hoke, E. T.; Shukla, P. K.; Risko, C.; Brédas, J.-L.; McGehee, M. D.; Beaujuge, P. M. Ring Substituents Mediate the Morphology of PBDTTPD-PCBM Bulk-Heterojunction Solar Cells. *Chem. Mater.* **2014**, *26*, 2299−2306.
(43) Bartelt, J. A.; Douglas, J. D.; Mateker, W. R.; Labban, A. E.; Tassone, C. J.; Toney, M. F.; Fréchet, J. M. J.; Beaujuge, P. M.; McGehee, M. D. Controlling Solution-Phase Polymer Aggregation with Molecular Weight and Solvent Additives to Optimize Polymer-Fullerene Bulk Heterojunction Solar Cells. *Adv. Energy Mater.* **2014**, *4*, 1301733.
(44) Ye, L.; Zhang, S.; Huo, L.; Zhang, M.; Hou, J. Molecular Design toward Highly Efficient Photovoltaic Polymers Based on Two-Dimensional Conjugated Benzodithiophene. *Acc. Chem. Res.* **2014**, *47*, 1595−1603.
(45) Huo, L.; Zhang, S.; Guo, X.; Xu, F.; Li, Y.; Hou, J. Replacing Alkoxy Groups with Alkylthienyl Groups: A Feasible Approach To Improve the Properties of Photovoltaic Polymers. *Angew. Chem.* **2011**, *123*, 9871−9876.
(46) Cowan, S. R.; Roy, A.; Heeger, A. J. Recombination in polymer-fullerene bulk heterojunction solar cells. *Phys. Rev. B: Condens. Matter Mater. Phys.* **2010**, *82*, 245207.
(47) Li, K.; Li, L.; Campbell, J. C. Recombination lifetime of free polarons in polymer/fullerene bulk heterojunction solar cells. *J. Appl. Phys.* **2012**, *111*, 034503.
(48) Blom, P. W. M.; Mihailetchi, V. D.; Koster, L. J. A.; Markov, D. E. Device Physics of Polymer:Fullerene Bulk Heterojunction Solar Cells. *Adv. Mater.* **2007**, *19*, 1551−1566.
(49) Kang, T. E.; Cho, H.-H.; Cho, C.-H.; Kim, K.-H.; Kang, H.; Lee, M.; Lee, S.; Kim, B.; Im, C.; Kim, B. J. Photoinduced Charge Transfer in Donor−Acceptor (DA) Copolymer: Fullerene Bis-adduct Polymer Solar Cells. *ACS Appl. Mater. Interfaces* **2013**, *5*, 861−868.
(50) Rivnay, J.; Mannsfeld, S. C. B.; Miller, C. E.; Salleo, A.; Toney, M. F. Quantitative Determination of Organic Semiconductor Micro-

DOI: 10.1021/acs.chemmater.7b03495
Chem. Mater. 2017, 29, 9407−9415

structure from the Molecular to Device Scale. *Chem. Rev.* **2012**, *112*, 5488−5519.
(51) Chen, M. S.; Niskala, J. R.; Unruh, D. A.; Chu, C. K.; Lee, O. P.; Fréchet, J. M. J. Control of Polymer-Packing Orientation in Thin Films through Synthetic Tailoring of Backbone Coplanarity. *Chem. Mater.* **2013**, *25*, 4088−4096.
(52) Kim, K.-H.; Park, S.; Yu, H.; Kang, H.; Song, I.; Oh, J. H.; Kim, B. J. Determining Optimal Crystallinity of Diketopyrrolopyrrole-Based Terpolymers for Highly Efficient Polymer Solar Cells and Transistors. *Chem. Mater.* **2014**, *26*, 6963−6970.
(53) Piliego, C.; Holcombe, T. W.; Douglas, J. D.; Woo, C. H.; Beaujuge, P. M.; Fréchet, J. M. J. Synthetic Control of Structural Order in N-Alkylthieno[3,4-c]pyrrole-4,6-dione-Based Polymers for Efficient Solar Cells. *J. Am. Chem. Soc.* **2010**, *132*, 7595−7597.
(54) Steyrleuthner, R.; Schubert, M.; Jaiser, F.; Blakesley, J. C.; Chen, Z.; Facchetti, A.; Neher, D. Bulk Electron Transport and Charge Injection in a High Mobility n-Type Semiconducting Polymer. *Adv. Mater.* **2010**, *22*, 2799−2803.
(55) Rivnay, J.; Steyrleuthner, R.; Jimison, L. H.; Casadei, A.; Chen, Z.; Toney, M. F.; Facchetti, A.; Neher, D.; Salleo, A. Drastic Control of Texture in a High Performance n-Type Polymeric Semiconductor and Implications for Charge Transport. *Macromolecules* **2011**, *44*, 5246−5255.
(56) Jiao, X.; Ye, L.; Ade, H. Quantitative Morphology−Performance Correlations in Organic Solar Cells: Insights from Soft X-Ray Scattering. *Adv. Energy Mater.* **2017**, *7*, 1700084.
(57) Collins, B. A.; Cochran, J. E.; Yan, H.; Gann, E.; Hub, C.; Fink, R.; Wang, C.; Schuettfort, T.; McNeill, C. R.; Chabinyc, M. L.; Ade, H. Polarized X-ray scattering reveals non-crystalline orientational ordering in organic films. *Nat. Mater.* **2012**, *11*, 536−543.
(58) Tumbleston, J. R.; Collins, B. A.; Yang, L.; Stuart, A. C.; Gann, E.; Ma, W.; You, W.; Ade, H. The influence of molecular orientation on organic bulk heterojunction solar cells. *Nat. Photonics* **2014**, *8*, 385−391.
(59) Liu, F.; Wang, C.; Baral, J. K.; Zhang, L.; Watkins, J. J.; Briseno, A. L.; Russell, T. P. Relating Chemical Structure to Device Performance via Morphology Control in Diketopyrrolopyrrole-Based Low Band Gap Polymers. *J. Am. Chem. Soc.* **2013**, *135*, 19248−19259.
(60) Holcombe, T. W.; Norton, J. E.; Rivnay, J.; Woo, C. H.; Goris, L.; Piliego, C.; Griffini, G.; Sellinger, A.; Brédas, J.-L.; Salleo, A.; Fréchet, J. M. J. Steric Control of the Donor/Acceptor Interface: Implications in Organic Photovoltaic Charge Generation. *J. Am. Chem. Soc.* **2011**, *133*, 12106−12114.
(61) Mukherjee, S.; Proctor, C. M.; Bazan, G. C.; Nguyen, T.-Q.; Ade, H. Significance of Average Domain Purity and Mixed Domains on the Photovoltaic Performance of High-Efficiency Solution-Processed Small-Molecule BHJ Solar Cells. *Adv. Energy Mater.* **2015**, *5*, 1500877.
(62) Ma, W.; Tumbleston, J. R.; Wang, M.; Gann, E.; Huang, F.; Ade, H. Domain Purity, Miscibility, and Molecular Orientation at Donor/Acceptor Interfaces in High Performance Organic Solar Cells: Paths to Further Improvement. *Adv. Energy Mater.* **2013**, *3*, 864−872.
(63) Mukherjee, S.; Proctor, C. M.; Tumbleston, J. R.; Bazan, G. C.; Nguyen, T.-Q.; Ade, H. Importance of Domain Purity and Molecular Packing in Efficient Solution-Processed Small-Molecule Solar Cells. *Adv. Mater.* **2015**, *27*, 1105−1111.
(64) Collins, B. A.; Li, Z.; Tumbleston, J. R.; Gann, E.; McNeill, C. R.; Ade, H. Absolute Measurement of Domain Composition and Nanoscale Size Distribution Explains Performance in PTB7:PC71BM Solar Cells. *Adv. Energy Mater.* **2013**, *3*, 65−74.
(65) Liu, Y.; Zhao, J.; Li, Z.; Mu, C.; Ma, W.; Hu, H.; Jiang, K.; Lin, H.; Ade, H.; Yan, H. Aggregation and morphology control enables multiple cases of high-efficiency polymer solar cells. *Nat. Commun.* **2014**, *5*, 5293.

DOI: 10.1021/acs.chemmater.7b03495
Chem. Mater. 2017, 29, 9407−9415